Supplementary Figure S1

A

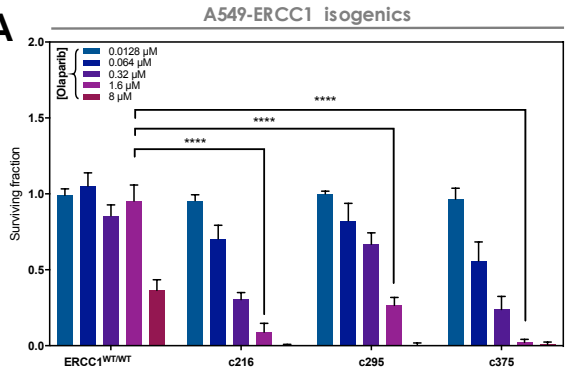

B *Top 50 downregulated REACTOME pathways in ERCC1$^{-/-}$ cells*

REACTOME pathways	*NES*	*Adjusted P value*
REACTOME_PROCESSING_OF_CAPPED_INTRON_CONTAINING_PRE_MRNA	-2.326	0.006
REACTOME_MRNA_PROCESSING	-2.312	0.006
REACTOME_MITOTIC_PROMETAPHASE	**-2.282**	**0.006**
REACTOME_MITOTIC_M_M_G1_PHASES	**-2.267**	**0.006**
REACTOME_MRNA_SPLICING	-2.242	0.006
REACTOME_DNA_REPLICATION	**-2.228**	**0.006**
REACTOME_CELL_CYCLE_MITOTIC	**-2.211**	**0.007**
REACTOME_ACTIVATION_OF_ATR_IN_RESPONSE_TO_REPLICATION_STRESS	**-2.174**	**0.006**
REACTOME_CELL_CYCLE	**-2.154**	**0.007**
REACTOME_TRANSPORT_OF_MATURE_TRANSCRIPT_TO_CYTOPLASM	-2.130	0.006
REACTOME_G2_M_CHECKPOINTS	**-2.088**	**0.006**
REACTOME_ACTIVATION_OF_THE_PRE_REPLICATIVE_COMPLEX	**-2.066**	**0.006**
REACTOME_E2F_MEDIATED_REGULATION_OF_DNA_REPLICATION	**-2.052**	**0.006**
REACTOME_CLEAVAGE_OF_GROWING_TRANSCRIPT_IN_THE_TERMINATION_REGION_	-2.033	0.006
REACTOME_MRNA_3_END_PROCESSING	-2.008	0.006
REACTOME_DNA_STRAND_ELONGATION	**-1.983**	**0.006**
REACTOME_METABOLISM_OF_NON_CODING_RNA	-1.970	0.006
REACTOME_GLYCOLYSIS	-1.946	0.006
REACTOME_TRANSPORT_OF_MATURE_MRNA_DERIVED_FROM_AN_INTRONLESS_TRANSCRIPT	-1.928	0.006
REACTOME_MRNA_SPLICING_MINOR_PATHWAY	-1.906	0.006
REACTOME_MITOTIC_G1_G1_S_PHASES	**-1.905**	**0.006**
REACTOME_CHROMOSOME_MAINTENANCE	**-1.905**	**0.006**
REACTOME_EXTENSION_OF_TELOMERES	-1.884	0.007
REACTOME_RNA_POL_II_TRANSCRIPTION	-1.861	0.006
REACTOME_G1_S_TRANSITION	**-1.828**	**0.006**
REACTOME_TRANSPORT_OF_RIBONUCLEOPROTEINS_INTO_THE_HOST_NUCLEUS	-1.820	0.014
REACTOME_M_G1_TRANSITION	**-1.816**	**0.006**
REACTOME_G1_S_SPECIFIC_TRANSCRIPTION	-1.813	0.021
REACTOME_INTERACTIONS_OF_VPR_WITH_HOST_CELLULAR_PROTEINS	-1.806	0.018
REACTOME_NEP_NS2_INTERACTS_WITH_THE_CELLULAR_EXPORT_MACHINERY	-1.796	0.014
REACTOME_PREFOLDIN_MEDIATED_TRANSFER_OF_SUBSTRATE_TO_CCT_TRIC	-1.795	0.020
REACTOME_CDC6_ASSOCIATION_WITH_THE_ORC_ORIGIN_COMPLEX	-1.781	0.020
REACTOME_ASSOCIATION_OF_LICENSING_FACTORS_WITH_THE_PRE_REPLICATIVE_COMPLEX	-1.777	0.019
REACTOME_REGULATION_OF_GLUCOKINASE_BY_GLUCOKINASE_REGULATORY_PROTEIN	-1.776	0.017
REACTOME_GLUCOSE_METABOLISM	-1.766	0.007
REACTOME_BASIGIN_INTERACTIONS	-1.757	0.037
REACTOME_TRANSCRIPTION_COUPLED_NER_TC_NER	**-1.752**	**0.010**
REACTOME_FORMATION_OF_TUBULIN_FOLDING_INTERMEDIATES_BY_CCT_TRIC	-1.749	0.041
REACTOME_LAGGING_STRAND_SYNTHESIS	**-1.748**	**0.036**
REACTOME_HIV_LIFE_CYCLE	-1.746	0.006
REACTOME_SYNTHESIS_OF_DNA	**-1.746**	**0.008**
REACTOME_ASSEMBLY_OF_THE_PRE_REPLICATIVE_COMPLEX	**-1.738**	**0.010**
REACTOME_NUCLEOTIDE_EXCISION_REPAIR	**-1.728**	**0.010**
REACTOME_S_PHASE	**-1.723**	**0.006**
REACTOME_PROCESSING_OF_CAPPED_INTRONLESS_PRE_MRNA	-1.712	0.041
REACTOME_E2F_ENABLED_INHIBITION_OF_PRE_REPLICATION_COMPLEX_FORMATION	**-1.701**	**0.041**
REACTOME_MITOTIC_G2_G2_M_PHASES	**-1.700**	**0.011**
REACTOME_CYCLIN_A_B1_ASSOCIATED_EVENTS_DURING_G2_M_TRANSITION	**-1.690**	**0.062**
REACTOME_KINESINS	-1.686	0.056

Cell cycle *DNA replication* *DNA repair*

C *Top 50 upregulated REACTOME pathways in ERCC1$^{-/-}$ cells*

REACTOME pathways	*NES*	*Adjusted P value*
REACTOME_INTERFERON_ALPHA_BETA_SIGNALING	**2.109**	**0.006**
REACTOME_ANTIGEN_PRESENTATION_FOLDING_ASSEMBLY_AND_PEPTIDE_LOADING_OF_CLASS_I_MHC	**1.957**	**0.006**
REACTOME_INNATE_IMMUNE_SYSTEM	**1.912**	**0.006**
REACTOME_INTERFERON_GAMMA_SIGNALING	**1.879**	**0.006**
REACTOME_INTERFERON_SIGNALING	**1.830**	**0.006**
REACTOME_IMMUNOREGULATORY_INTERACTIONS_BETWEEN_A_LYMPHOID_AND_A_NON_LYMPHOID_CELL	**1.827**	**0.007**
REACTOME_CHEMOKINE_RECEPTORS_BIND_CHEMOKINES	**1.817**	**0.006**
REACTOME_CYTOKINE_SIGNALING_IN_IMMUNE_SYSTEM	**1.786**	**0.006**
REACTOME_NEGATIVE_REGULATORS_OF_RIG_I_MDA5_SIGNALING	**1.758**	**0.017**
REACTOME_COMPLEMENT_CASCADE	**1.752**	**0.020**
REACTOME_REGULATION_OF_COMPLEMENT_CASCADE	**1.730**	**0.017**
REACTOME_KERATAN_SULFATE_KERATIN_METABOLISM	1.684	0.041
REACTOME_RIG_I_MDA5_MEDIATED_INDUCTION_OF_IFN_ALPHA_BETA_PATHWAYS	**1.647**	**0.020**
REACTOME_KERATAN_SULFATE_BIOSYNTHESIS	1.629	0.075
REACTOME_TRAF6_MEDIATED_NFKB_ACTIVATION	**1.626**	**0.076**
REACTOME_TOLL_RECEPTOR_CASCADES	**1.597**	**0.020**
REACTOME_TRANSPORT_OF_GLUCOSE_AND_OTHER_SUGARS_BILE_SALTS_AND_ORGANIC_ACIDS_METAL_IONS_AND_AMINE_COMPOUNDS	1.595	0.049
REACTOME_NOD1_2_SIGNALING_PATHWAY	1.591	0.076
REACTOME_TRAF3_DEPENDENT_IRF_ACTIVATION_PATHWAY	**1.581**	**0.097**
REACTOME_IL_3_5_AND_GM_CSF_SIGNALING	**1.575**	**0.075**
REACTOME_O_LINKED_GLYCOSYLATION_OF_MUCINS	1.575	0.074
REACTOME_TERMINATION_OF_O_GLYCAN_BIOSYNTHESIS	1.553	0.111
REACTOME_NUCLEOTIDE_BINDING_DOMAIN_LEUCINE_RICH_REPEAT_CONTAINING_RECEPTOR_NLR_SIGNALING_PATHWAYS	1.553	0.091
REACTOME_ASPARAGINE_N_LINKED_GLYCOSYLATION	1.550	0.045
REACTOME_N_GLYCAN_TRIMMING_IN_THE_ER_AND_CALNEXIN_CALRETICULIN_CYCLE	1.545	0.123
REACTOME_IL_RECEPTOR_SHC_SIGNALING	**1.531**	**0.146**
REACTOME_PEPTIDE_LIGAND_BINDING_RECEPTORS	1.528	0.091
REACTOME_AMYLOIDS	1.525	0.106
REACTOME_IL_2_SIGNALING	**1.521**	**0.111**
REACTOME_ACTIVATION_OF_CHAPERONE_GENES_BY_XBP1S	1.514	0.091
REACTOME_ANTIGEN_PROCESSING_CROSS_PRESENTATION	1.505	0.086
REACTOME_INSULIN_SYNTHESIS_AND_PROCESSING	1.500	0.162
REACTOME_METAL_ION_SLC_TRANSPORTERS	1.491	0.183
REACTOME_ACTIVATION_OF_IRF3_IRF7_MEDIATED_BY_TBK1_IKK_EPSILON	**1.484**	**0.183**
REACTOME_RIP_MEDIATED_NFKB_ACTIVATION_VIA_DAI	**1.481**	**0.183**
REACTOME_SIGNALING_BY_ILS	1.481	0.071
REACTOME_CALNEXIN_CALRETICULIN_CYCLE	1.479	0.183
REACTOME_ACTIVATION_OF_CHAPERONES_BY_ATF6_ALPHA	1.478	0.183
REACTOME_ZINC_TRANSPORTERS	1.476	0.186
REACTOME_RAP1_SIGNALLING	1.473	0.192
REACTOME_TRIF_MEDIATED_TLR3_SIGNALING	**1.434**	**0.129**
REACTOME_TRAF6_MEDIATED_IRF7_ACTIVATION	**1.430**	**0.237**
REACTOME_ACTIVATED_TLR4_SIGNALLING	**1.428**	**0.108**
REACTOME_UNFOLDED_PROTEIN_RESPONSE	1.423	0.123
REACTOME_ERK_MAPK_TARGETS	1.413	0.243
REACTOME_SIGNALING_BY_FGFR1_FUSION_MUTANTS	1.409	0.251
REACTOME_PHASE1_FUNCTIONALIZATION_OF_COMPOUNDS	1.381	0.250
REACTOME_DIABETES_PATHWAYS	1.380	0.123
REACTOME_NFKB_AND_MAP_KINASES_ACTIVATION_MEDIATED_BY_TLR4_SIGNALING_REPERTOIRE	**1.368**	**0.192**

Immune signaling *Antigen presentation* *PRR signaling*

D

Genes	*log$_2$ FC*	*FDR*
Interferon receptors		
IFNAR2	0.6988	6.11E-05
IFNGR1	1.5014	1.15E-10
IFNGR2	0.8441	7.54E-08
Signal transducers and activators of transcription (STAT)		
STAT1	-0.6777	1.56E-04
STAT2	0.6025	5.33E-05
STAT3	0.5017	1.26E-04
STAT5A	1.5612	1.01E-08
STAT5B	0.3163	1.40E-02
STAT6	0.9319	1.98E-05

E

Genes	*log$_2$ FC*	*FDR*
C-C motif cytokines		
CCL2	2.3992	1.01E-08
CCL5	7.4502	4.38E-09
CCL26	1.4605	5.16E-06
C-X-C motif cytokines		
CXCL1	6.7536	3.96E-11
CXCL2	5.3524	7.16E-09
CXCL3	4.9923	2.38E-10
CXCL5	3.2972	1.11E-14
CXCL8	6.0042	5.84E-14
CXCL10	6.0637	3.92E-05
CXCL16	0.7017	1.34E-05

Supplementary Figure S1, related to Figure 1. ERCC1-deficient NSCLC cells exhibit enhanced activation of immune signaling compared to their ERCC1-proficient counterparts. A, Assessment of Ola cytotoxicity in A549-ERCC1$^{WT/WT}$ vs A549-c216, -c295, and -c375 cell lines. Cells were treated with a dose range of Ola and exposed to the drug for 14 days, with drug-containing media replenishment every 2 days (colony-formation assay). Shown are surviving fractions; Mean ± SD, *N* = 4, two-way ANOVA, *post hoc* Dunnett's test. **B**, GSEA of REACTOME pathways in A549-ERCC1$^{-/-}$ cells compared with A549-ERCC1$^{WT/WT}$. Shown are the top 50 downregulated REACTOME pathways in A549-ERCC1$^{-/-}$ cells. Pathways highlighted in yellow relate to cell cycle; pathways highlighted in light green relate to DNA replication; pathways highlighted in dark green relate to DNA repair. **C**, GSEA of REACTOME pathways in A549-ERCC1$^{-/-}$ cells compared with A549-ERCC1$^{WT/WT}$. Shown are the top 50 upregulated REACTOME pathways in A549-ERCC1$^{-/-}$ cells. Pathways highlighted in pink relate to immune signaling; pathways highlighted in red relate to antigen presentation; pathways highlighted in brown relate to PRR signaling. **D,** Selective table showing differential expression of several IFN-inducible proteins including IFN receptors, and signal transducer and activator of transcription (STAT) members. **E,** Selective table showing differential expression of several chemoattractant chemokines, including members of the C-C and C-X-C motif cytokines families.

Abbreviations: DEGs, Differentially Expressed Genes; GSEA, Gene Set Enrichment Analysis; IFN, interferons; PRR, Pattern Recognition Receptors.

Supplementary Figure S2

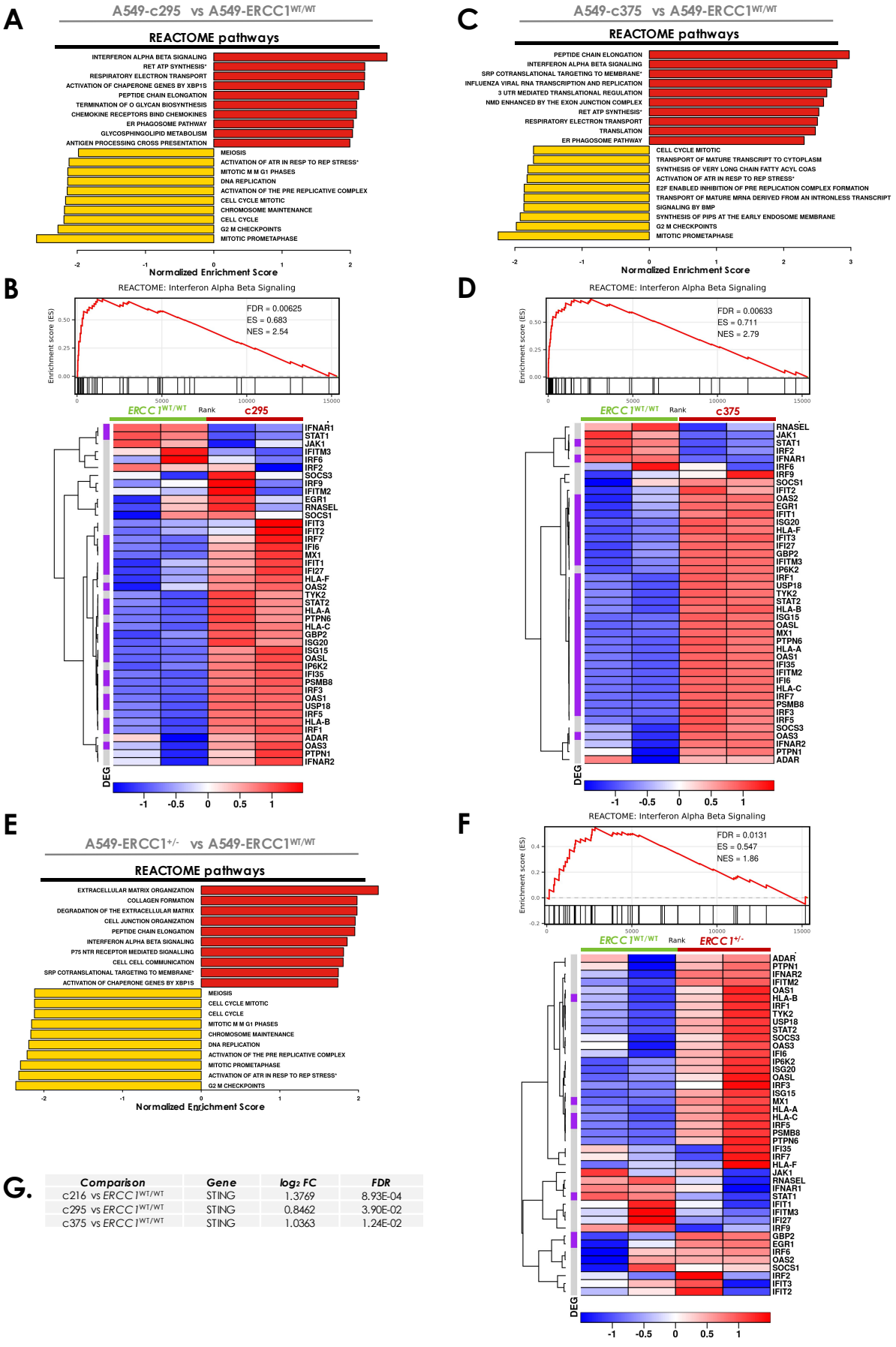

G.

Comparison	Gene	log2 FC	FDR
c216 vs *ERCC1*$^{WT/WT}$	STING	1.3769	8.93E-04
c295 vs *ERCC1*$^{WT/WT}$	STING	0.8462	3.90E-02
c375 vs *ERCC1*$^{WT/WT}$	STING	1.0363	1.24E-02

Supplementary Figure S2, related to Figure 1 and 2. Two other ERCC1-deficient A549 clones and the heterozygous A549-ERCC1$^{+/-}$ cell line exhibit enhanced activation of type I IFN signaling compared to the A549-ERCC1$^{WT/WT}$ cell line. A, GSEA of REACTOME pathways in A549-c295 cells compared with A549-ERCC1$^{WT/WT}$. Red, top 10 upregulated REACTOME pathways in A549-c295 cells; Yellow, top 10 downregulated REACTOME pathways A549-c295 cells. **B**, GSEA of the REACTOME pathway Interferon Alpha Beta Signaling in A549-c295 cells compared with A549-ERCC1$^{WT/WT}$, and associated heatmap showing genes of the pathway, ranked by FDR. *N* = 2; Heatmap scale is a Z score. Purple, significantly DEGs with FDR < 0.05 and |LFC| > 1; Grey, non-significantly DEGs. **C**, GSEA of REACTOME pathways in A549-c375 cells compared with A549-ERCC1$^{WT/WT}$. Red, top 10 upregulated REACTOME pathways in A549-c375 cells; Yellow, top 10 downregulated REACTOME pathways A549-c375 cells. **D**, GSEA of the REACTOME pathway Interferon Alpha Beta Signaling in A549-c375 cells compared with A549-ERCC1$^{WT/WT}$, and associated heatmap showing genes of the pathway, ranked by FDR. *N* = 2; Heatmap scale is a Z score. Purple, significantly DEGs with FDR < 0.05 and |LFC| > 1; Grey, non-significantly DEGs. **E**, GSEA of REACTOME pathways in A549-ERCC1$^{+/-}$ cells compared with A549-ERCC1$^{WT/WT}$. Red, top 10 upregulated REACTOME pathways in A549-ERCC1$^{+/-}$ cells; Yellow, top 10 downregulated REACTOME pathways A549-ERCC1$^{+/-}$ cells. **F**, GSEA of the REACTOME pathway Interferon Alpha Beta Signaling in A549-ERCC1$^{+/-}$ cells compared with A549-ERCC1$^{WT/WT}$, and associated heatmap showing genes of the pathway, ranked by FDR. *N* = 2; Heatmap scale is a Z score. Purple, significantly DEGs with FDR < 0.05 and |LFC| > 1; Grey, non-significantly DEGs. **G,** Selective table showing differential expression of STING in A549-c216, -c295 and -c375 cells compared with A549-ERCC1$^{WT/WT}$ cells.

Abbreviations: DEGs, Differentially Expressed Genes; FDR, False Discovery Rate; GSEA, Gene Set Enrichment Analysis; LFC, $\log_2$(fold-change); NES, Normalized Enrichment Score.

Supplementary Figure S3

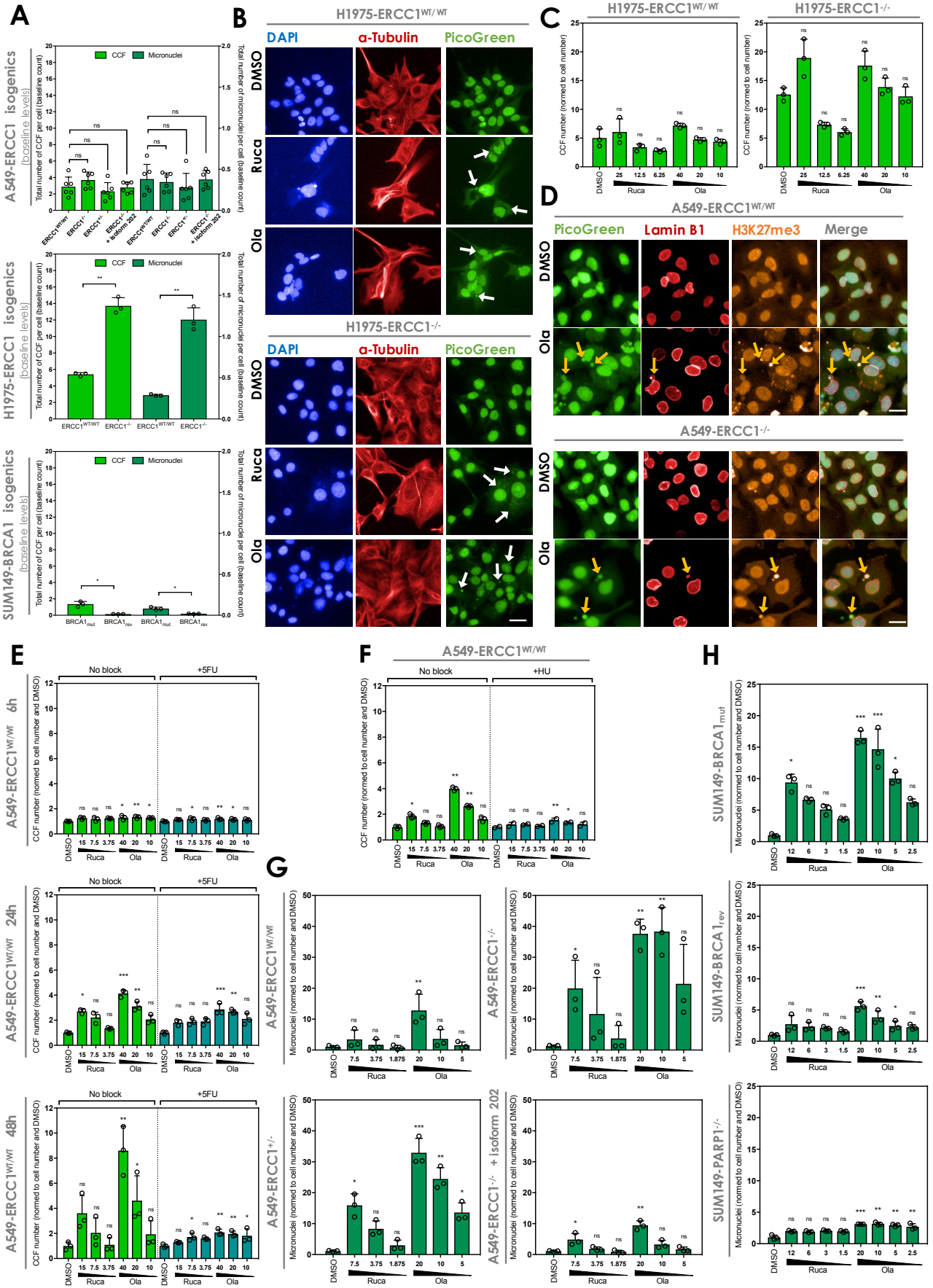

Supplementary Figure S3, related to Figure 3 and 4. PARPi-generated CCF have micronuclei characteristics. A, Automated quantification of baseline levels of CCF and micronuclei in A549-ERCC1$^{WT/WT}$, A549-ERCC1$^{-/-}$, A549-ERCC1$^{+/-}$, A549-ERCC1$^{-/-}$ + isoform 202, H1975-ERCC1$^{WT/WT}$, H1975-ERCC1$^{-/-}$, SUM149-BRCA1$_{mut}$ and SUM149-BRCA1$_{rev}$ cells, using Columbus software. Number of CCF per cell (left Y axis) or micronuclei per cell (right Y axis) are depicted. Mean ± SD, *N* = 3, Kruskal-Wallis test and *post hoc* Dunn's test or unpaired t test with Welch's correction. Results shown are representative of 2 experiments performed with similar results. **B**, Representative immunofluorescence images of DMSO-, Ruca- and Ola-exposed H1975-ERCC1$^{WT/WT}$ and H1975-ERCC1$^{-/-}$ cells. Blue, DAPI; Red, α-Tubulin; Green, PicoGreen. Cells were exposed to 25 μM Ruca or 40 μM Ola during 72h. White arrows, CCF. Scale bar, 20 μm. **C**, Automated quantification of CCF in H1975-ERCC1$^{WT/WT}$ and H1975-ERCC1$^{-/-}$ cells exposed to increasing doses of Ruca or Ola, using Columbus software. Number of CCF per cell is depicted. Mean ± SD, *N* = 3, Kruskal-Wallis test and *post hoc* Dunn's test, relative to DMSO control. **D**, Representative immunofluorescence images of DMSO- and Ola-exposed A549-ERCC1$^{WT/WT}$ and A549-ERCC1$^{-/-}$ cells. Green, PicoGreen; Red, Lamin B1; Orange, H3K27me3. Cells were exposed to 40 μM Ola or DMSO (vehicle) during 72h. Yellow arrows, micronuclei. Scale bar, 20 μm. **E**, Automated quantification of CCF at indicated timepoints in A549-ERCC1$^{WT/WT}$ cells exposed to increasing doses of Ruca or Ola (μM) in the presence or absence of the cell cycle blocker 5-fluorouracil. Number of CCF per cell, counted using Columbus software, are normalized to the DMSO (vehicle). Mean ± SD, *N* = 3, Kruskal-Wallis test and *post hoc* Dunn's test, relative to DMSO control. **F**, Automated quantification of CCF in A549-ERCC1$^{WT/WT}$ cells exposed to increasing doses of Ruca or Ola (μM) during 48h in the presence or absence of the cell cycle blocker hydroxyurea. Number of CCF per cell, counted using Columbus software, are normalized to the DMSO (vehicle). Mean ± SD, *N* = 3, Kruskal-Wallis test and *post hoc* Dunn's test, relative to DMSO control. **G**, Automated quantification of micronuclei in A549-ERCC1 isogenic cells exposed to increasing doses of Ruca or Ola (μM), using Columbus software. Number of micronuclei per cell normalized to the DMSO (vehicle) of the corresponding cell line is depicted. Mean ± SD, *N* = 3, Kruskal-Wallis test and *post hoc* Dunn's test, relative to DMSO control. Results shown are representative of 2 experiments performed with similar results. **H**, Automated quantification

of micronuclei in SUM149-BRCA1$_{mut}$, SUM149-BRCA1$_{rev}$ and SUM149-PARP1$^{-/-}$ cells exposed to increasing doses of Ruca or Ola (μM), using Columbus software. Number of micronuclei per cell normalized to the DMSO (vehicle) of the corresponding cell line is depicted. Mean ± SD, *N* = 3, Kruskal-Wallis test and *post hoc* Dunn's test, relative to DMSO control. Results shown are representative of 2 experiments performed with similar results. Abbreviations: 5-FU, 5-fluorouracil; HU, hydroxyurea; Ola, olaparib; Ruca, rucaparib. SD, Standard Deviation;

Supplementary Figure S4

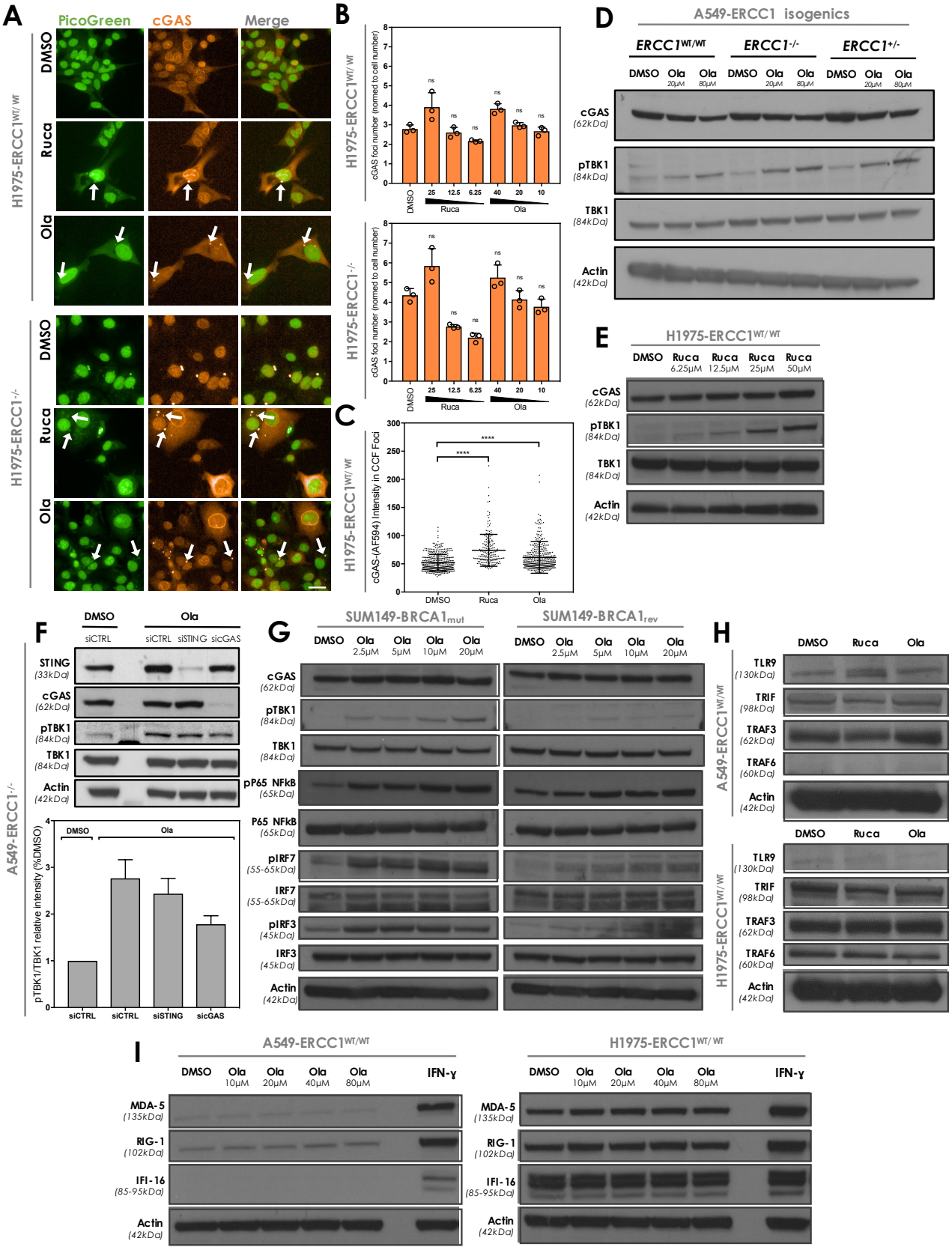

Supplementary Figure S4, related to Figure 5 and 6. PARPi activate STING signaling through cGAS-mediated detection of CCF. A, Representative immunofluorescence images of DMSO-, Ruca- and Ola-exposed H1975-ERCC1$^{WT/WT}$ and H1975-ERCC1$^{-/-}$ cells. Green, PicoGreen; Orange, cGAS. Cells were exposed to 25 μM Ruca or 40 μM Ola during 72h. White arrows, CCF. Scale bar, 20 μm. Images corresponding to the Ruca condition originate from the same image field as those displayed in Supplementary Figure S3B. **B**, Automated quantification of cytoplasmic cGAS foci in H1975-ERCC1$^{WT/WT}$ and H1975-ERCC1$^{-/-}$ cells exposed to increasing doses of Ruca or Ola (μM), using Columbus software. Number of cytoplasmic cGAS foci per cell is depicted. Mean ± SD, *N* = 3, Kruskal-Wallis test and *post hoc* Dunn's test, relative to DMSO control. **C**, Scatter box plots displaying cGAS foci intensity for each co-localizing CCF foci in H1975-ERCC1$^{WT/WT}$ cells exposed to DMSO (vehicle), 25 μM Ruca or 40 μM Ola. *N* = 3, Kruskal-Wallis test and *post hoc* Dunn's test. **D**, Western blot of phospho-TBK1 in A549-ERCC1$^{WT/WT}$, A549-ERCC1$^{+/-}$ and A549-ERCC1$^{-/-}$ cells upon PARPi exposure. Cells were exposed to DMSO (vehicle), 20 μM or 80 μM Ola for 48h, and lysates were probed with the indicated antibodies. **E**, Western blot of phospho-TBK1 in H1975-ERCC1$^{WT/WT}$ cells upon PARPi exposure. Cells were exposed to DMSO (vehicle), or a dose range of Ruca for 48h, and lysates were probed with the indicated antibodies. **F**, Western blot of phospho-TBK1 in DMSO- or Ola-treated A549-ERCC1$^{-/-}$ cells in the context of siRNA silencing of cGAS or STING. Cells were transfected with siCTRL, siSTING or sicGAS, exposed to DMSO (vehicle) or 40 μM Ola, and lysates were probed with the indicated antibodies. Bar plot: pTBK1 intensity was measured for each condition. **G**, Western blot showing phosphorylation levels of several downstream STING signaling effectors in SUM149-BRCA1$_{mut}$ and SUM149-BRCA1$_{rev}$ cells exposed to DMSO (vehicle) or a dose range of Ola for 48h. Lysates were probed with the indicated antibodies. **H**, **I**, Western Blot showing protein expression of several TLR (**H**) or RLR (**I**) effectors in A549-ERCC1$^{WT/WT}$ and H1975-ERCC1$^{WT/WT}$ cells exposed to DMSO (vehicle) or a dose range of Ola for 48h. Lysates were probed with the indicated antibodies and IFNγ was used as a positive control of activation. Abbreviations: Ola, olaparib; RLR, RIG-I-like receptors; Ruca, rucaparib; SD, Standard Deviation; TLR, Toll-like receptors.

Supplementary Figure S5

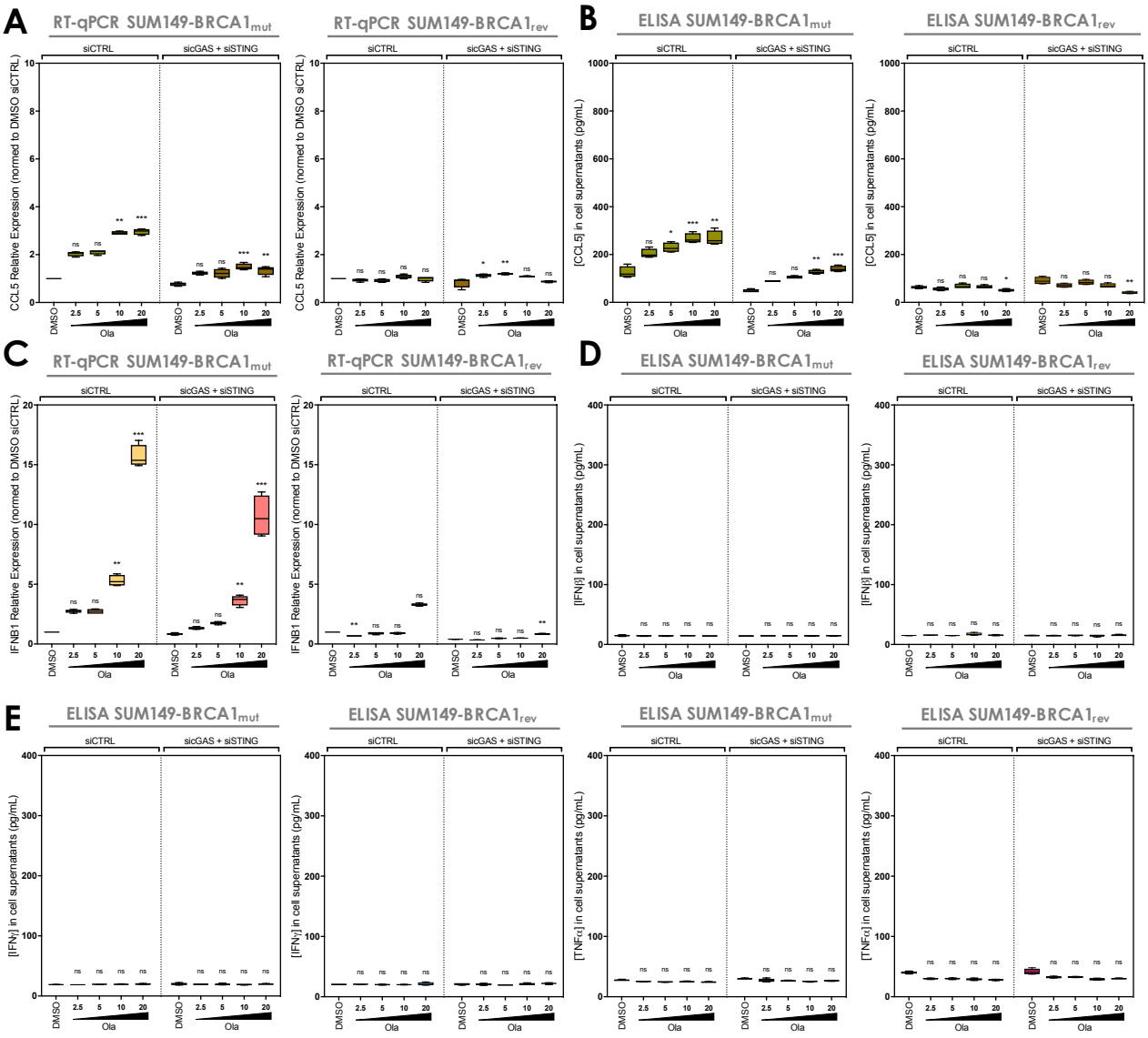

Supplementary Figure S5, related to Figure 7. PARPi activate CCL5 transcription and secretion in BRCA1-defective cells. A, RT-qPCR analysis of RNA isolated from Ola-exposed SUM149-BRCA1$_{mut}$ and SUM149-BRCA1$_{rev}$ cells, in the presence or absence of cGAS/STING silencing by siRNA. Cells were transfected with siCTRL or sicGAS + siSTING and treated for 72h with DMSO or a dose range of Ola (μM). CCL5 mRNAs were analyzed relative to GAPDH (to control for cDNA quantity). Box-and-whisker plots show arbitrary units of gene expression, normalized to DMSO-treated control. Boxes indicate median, lower and upper quartiles; Whiskers indicate the 5th to 95th percentile range; *N* = 4, Kruskal-Wallis test and *post hoc* Dunn's test, relative to DMSO control. **B**, Quantitative analysis of CCL5 secretion in SUM149-BRCA1$_{mut}$ and SUM149-BRCA1$_{rev}$ cells supernatants upon Ola exposure, in the presence or absence of cGAS/STING silencing by siRNA. Cells were transfected with siCTRL or sicGAS + siSTING and treated for 72h with DMSO or a dose range of Ola (μM). Supernatants were collected and analysed by ELISA for detection of CCL5. Box-and-whisker plots show CCL5 concentrations. Boxes indicate median, lower and upper quartiles; Whiskers indicate the 5th to 95th percentile range; *N* = 4, Kruskal-Wallis test and *post hoc* Dunn's test, relative to DMSO control. **C**, RT-qPCR analysis of RNA isolated from Ola-exposed SUM149-BRCA1$_{mut}$ and SUM149-BRCA1$_{rev}$ cells, in the presence or absence of cGAS/STING silencing by siRNA. Cells were transfected with siCTRL or sicGAS + siSTING and treated for 72h with DMSO or a dose range of Ola (μM). *IFNB1* mRNAs were analyzed relative to GAPDH (to control for cDNA quantity). Box-and-whisker plots show arbitrary units of gene expression, normalized to DMSO-treated control. Boxes indicate median, lower and upper quartiles; Whiskers indicate the 5th to 95th percentile range; *N* = 4, Kruskal-Wallis test and *post hoc* Dunn's test, relative to DMSO control. **D**, **E**, Quantitative analysis of IFN-β (**D**), IFN-γ and TNF-α (**E**) secretion in SUM149-BRCA1$_{mut}$ and SUM149-BRCA1$_{rev}$ cells supernatants on Ola exposure, in the presence or absence of cGAS/STING silencing by siRNA. Cells were transfected with siCTRL or sicGAS + siSTING and treated for 72h with DMSO or a dose range of Ola (μM). Supernatants were collected and analysed by ELISA for detection of IFN-β, IFN-γ and TNF-α. Box-and-whisker plots show IFN-β, IFN-γ or TNF-α concentrations. Boxes indicate median, lower and upper quartiles; Whiskers indicate the 5th to 95th percentile range; *N* = 4, Kruskal-Wallis test and *post hoc* Dunn's test, relative to DMSO control. Abbreviations: ELISA,

enzyme-linked immunosorbent assay; IFN, interferon; Ola, olaparib; SD, standard deviation; TNF, Tumor Necrosis Factor.

Supplementary Figure S6

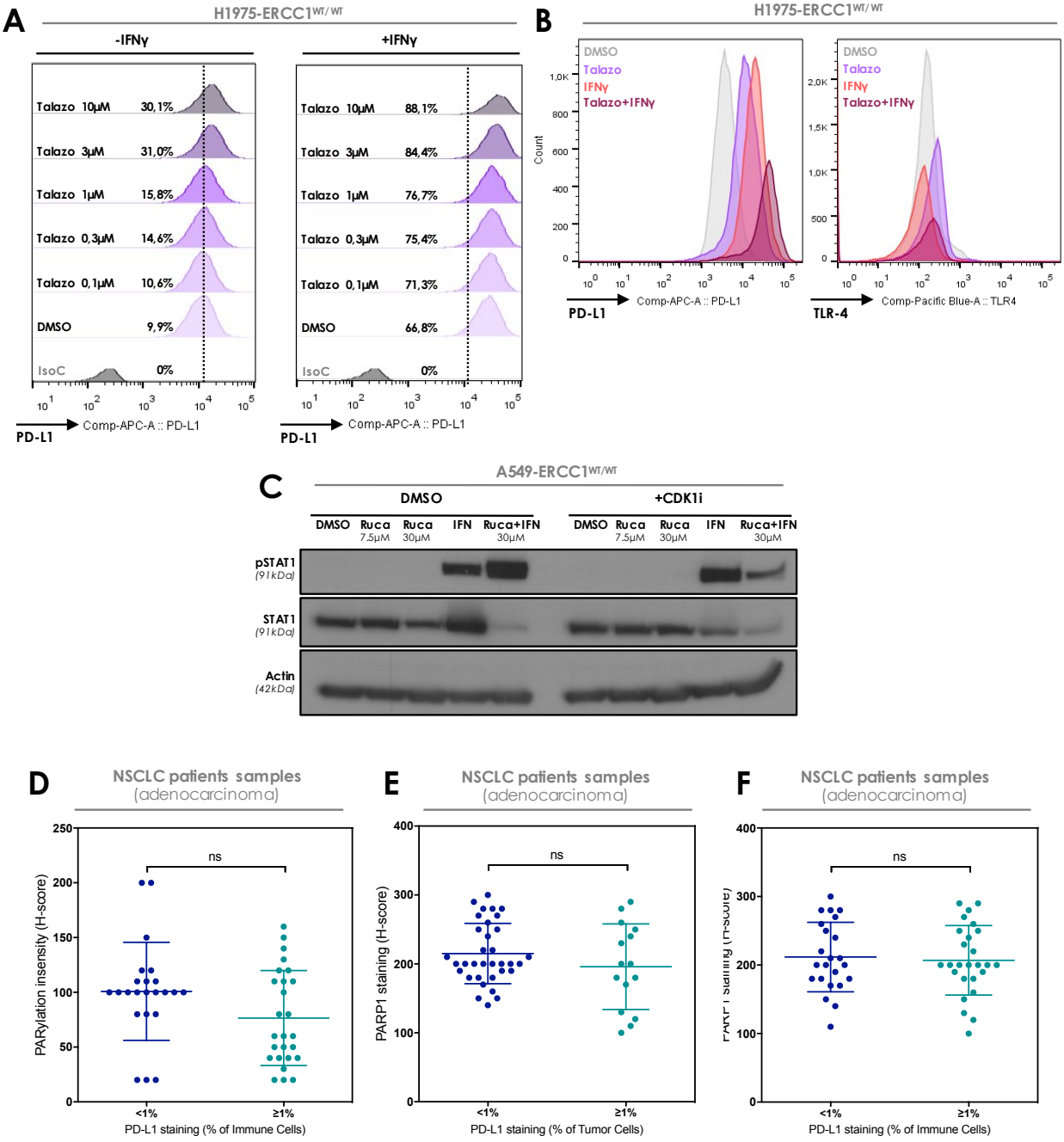

Supplementary Figure S6, related to Figure 8 and 9. PARPi-mediated upregulation of PD-L1 is dose-dependent, and associates with enhanced type II IFN signaling. A, Representative flow cytometry histograms showing PD-L1 expression in Talazo-treated H1975-ERCC1$^{WT/WT}$, in the presence or absence of IFNγ. Cells were treated with DMSO, or a dose range of Talazo, in combination or not with 500 Ui/mL IFNγ. Shown is the percentage of PD-L1-positive cells. **B**, Representative flow cytometry histograms showing PD-L1 and TLR4 expression in H1975-ERCC1$^{WT/WT}$ cells on PARPi exposure, in the presence or absence of IFNγ. Cells were treated with DMSO, 3 μM Talazo, 500 Ui/mL IFNγ or both. **C**, Western blot of phospho-STAT1 in A549-ERCC1$^{WT/WT}$ cells under Ruca and IFNγ exposure, in the presence or absence of the cell cycle blocker CDK1 inhibitor RO-3306. Cells were treated for 48h with DMSO, 7.5 μM Ruca, 30 μM Ruca, 500 Ui/mL IFNγ or a combination of Ruca and IFNγ, and lysates were probed with the indicated antibodies. **D**, Scatter box plot depicting the absence of correlation between the level of PARylation and the immune cell expression of PD-L1 (as assessed by IHC staining) in a series of resected stage 1 human NSCLC adenocarcinoma samples (n = 49); Mann-Whitney U test was applied. **E**, Scatter box plot depicting the absence of correlation between expression of PARP1 and tumor cell expression of PD-L1 (as assessed by IHC staining) in a series of resected stage 1 human NSCLC adenocarcinoma samples (n = 49); Mann-Whitney U test was applied. **F**, Scatter box plot depicting the absence of correlation between expression of PARP1 and immune cell expression of PD-L1 (as assessed by IHC staining) in a series of resected stage 1 human NSCLC adenocarcinoma samples (n = 49); Mann-Whitney U test was applied. Abbreviations: CDK1i, CDK1 inhibitor; MFI, Mean Fluorescence Intensity; Nira, niraparib; Ola, olaparib; Ruca, rucaparib; Talazo, talazoparib.

Additional Methods

Antibodies

For immunoblotting and immunofluorescence applications, antibodies targeting the following epitopes were used: STING (#13647), cGAS (#15102), pTBK1 (#5483), TBK1 (#3013), pNF-κB P65 (#3033), NF-κB P65 (#8242), pIRF7 (#12390), IRF7 (#4920), pIRF3 (#4947), IRF3 (#4302), pSTAT1 (#9167), STAT1 (#9176), PD-L1 (#13684), RIG-1 (#3743), MDA-5 (#5321), TLR9 (#13674), TRIF (#4596), TRAF3 (#4729), and TRAF6 (#8028) from Cell Signalling Technology (Danvers, MA, USA); Histone H3 (ab1791), Histone H3 tri-methyl-K27 (ab6002), α-Tubulin (ab7291) and Lamin B1 (ab8982) from Abcam (Cambridge, UK); IFI16 (sc-8023) and ERCC1 (sc-17809) from Santa Cruz (Dallas, TX, USA); β-Actin (A1978) from Sigma-Aldrich (Gillingham, UK). For flow cytometry applications, the following antibodies were used: APC-conjugated anti-human CD274 (#329708), and APC-conjugated mouse IgG2b, κ isotype control (#400322), from BioLegend (San Diego, CA, USA); BV421-conjugated mouse anti-human CD284 (#564401) and BV421-conjugated mouse IgG1, κ Isotype Control (#562438) from BD Biosciences (San Jose, CA, USA). For immunohistochemistry (IHC) applications, the following antibodies were used: ERCC1 SP68 (M3680) from Spring Bioscience (Pleasanton, CA, USA), PAR (MABC547) from Merck Millipore (Burlington, MA, USA), PARP1 (MCA1522G) from BioRad (Hercules, CA, USA), and PD-L1 (#13684) from Cell Signalling Technology.

RNAi and transfections

All siRNA silencing experiments were performed using a pre-designed ON-TARGETplus SMARTpool (Dharmacon, Lafayette, CO, USA) of four distinct siRNA species targeting different sequences of the target transcript: cGAS, ON-TARGETplus MB21D1 siRNA (L-015607-02-0005); STING, ON-TARGETplus TMEM173 siRNA (L-024333-02-0005). Cells were plated at medium density in 6-well plates and transfected 24 h after seeding using RNAimax (Invitrogen) transfection reagent. Transfection efficacy was assessed through concomitant but independent transfection of cells with PLK1 siRNA, which produced more

than 95% cell growth inhibition. Validation of siRNA gene silencing was performed via western blotting from pools of concomitantly transfected cells.

Cell-based survival assays

Short-term survival assays were performed in 96-well plates. Exponentially growing cells were plated at a concentration of 1000 cells/well. Drug was added 24 h after seeding and cells were continuously exposed to the drug for 5 days, after which cell viability was estimated using CellTiter-Glo® luminescence (Promega, Madison, WI, USA) on a Victor multilabel plate reader (PerkinElmer, Waltham, MA, USA), and survival fractions were calculated compared to the DMSO-treated control.

Colony-formation assays were performed in 6-well plates. Exponentially growing cells were plated at a concentration of 500 cells/well. Drug was added 24 h after seeding and cells were exposed to the drug for 14 days, with drug-containing media replenishment every 2 days. Cells were then fixed with 10% trichloroacetic acid and stained with sulphorhodamine B (Sigma-Aldrich, Gillingham, UK). Colonies were counted manually and using a colony counting machine (ColCount, Oxford Optronix, Abingdon, UK). Survival fractions were calculated compared to the DMSO-treated control.

Image analysis for CCF/micronuclei identification

Micronuclei and CCF were assessed using an automated quantification with the Columbus software, and distinguished based on staining intensity following manufacturer's recommendations. A micronucleus was defined as a small region of the image having a Picogreen staining intensity > 20% higher than the surrounding cytoplasm; CCF were defined as small regions displaying higher intensity than the surrounding cytoplasm but at an intensity around the sensitivity threshold (i.e. lower than the micronuclei threshold). CCF were identified after the application of (i) a background correction and (ii) a splitting coefficient (to enable the separation of connected foci).

Immunoblotting

Cells were lysed in RIPA lysis and extraction buffer (Thermo Fisher Scientific, Waltham, MA, USA) supplemented with 0.5% phenylmethylsulfonyl fluoride (PMSF) and 1% Halt™ protease and phosphatase inhibitor cocktail (Thermo Fisher Scientific). Lysates were generated on ice, and centrifuged 10min at 16,900g prior to supernatant collection. Supernatants were then subjected to electrophoresis using NuPAGE™ 4-12% Bis-Tris precast gels (Invitrogen, Carlsbad, CA, USA). After migration, proteins were transferred to a nitrocellulose membrane (GE Healthcare). 5% bovine serum albumin (BSA) in TBS buffer supplemented with 0.1% Tween 20 (TBST) was used to block the membrane, at room temperature (RT) for 1 h. Primary antibodies were diluted in 5% BSA in TBST, and incubated at 4°C overnight. The next day, the membrane was washed three times with TBST, each for 10 min, followed by incubation with horseradish-peroxidase-conjugated secondary antibodies at RT for 1 h, in 5% milk in TBST. The membrane was washed again three times with TBST, and incubated with Amersham ECL prime detection reagent (GE Healthcare). The membrane was then exposed to X-ray film and the film developed in a darkroom.

RT-qPCR

RNA from cells was extracted using the RNeasy mini kit (Qiagen, Venlo, Netherlands), quantified with a NanoDrop™ 2000 spectrophotometer (Thermo Fisher Scientific) and diluted to equal concentrations across all samples. Reverse transcription was performed using a SuperScript® VILO™ cDNA synthesis kit (Invitrogen), following the manufacturer's protocol. The qPCR was performed using a QuantStudio 6 Flex Real-Time PCR system with TaqMan™ Fast Advanced master mix (Thermo Fisher Scientific). The following primers were used for the RT-qPCR: IFNB1 TaqMan® gene expression assay (Hs01077958_s1), CCL5 TaqMan® gene expression assay (Hs00982282_m1), CD274 TaqMan® gene expression assay (Hs00204257_m1) and GAPDH TaqMan® gene expression assay (Hs03929097_g1). Results were normalized to GAPDH.

Immunohistochemistry and pathological scoring

Archival samples from resected NSCLC (invasive adenocarcinomas and squamous cell carcinomas) were used. For each patient sample, a single representative formalin-fixed paraffin embedded (FFPE) block was selected for the study. FFPE blocks were sectioned (4 µm thick) on a RM2245 microtome (Leica Biosystems) and placed onto histological Polysine™ microscope adhesion slides (Thermo Fisher Scientific). For PAR, PARP1 and ERCC1 stainings, tissue sections were deparaffinized in xylene rehydrated by incubation in serial ethanol baths (95%, 70%, 50%, 30%, volume/volume in PBS, 2 min per bath). Epitope retrieval was performed through incubation in 10 mM citrate buffer (pH 6.0 or pH 7.3) for 30 to 40 min. Endogenous peroxidase activity was inhibited by treatment with peroxidase blocking reagent (Dako, Carpinteria, CA, USA). Unspecific binding sites were then blocked for 10 min with protein block reagent (Dako) and the slides were incubated for 1 h at RT with PAR (1:1500), PARP1 (1:4000) or ERCC1 (1:500) primary antibodies. After three washes in PBS, the slides were incubated for 30 min at RT with Vectastain Universal Elite ABC secondary antibody (Vector Laboratories Inc., Burlingame, MA, USA), and subsequently revealed by the streptavidin-biotin-peroxidase complex method with 3,3′-diaminobenzidine tetrahydrochloride (DAB) as chromogenic substrate. For PD-L1 staining, automated immunohistochemistry was performed using a Ventana Discovery Ultra platform (Ventana Medical Systems, Oro Valley, AZ, USA). After deparaffinization, and epitope retrieval using CC1 buffer (64 min at 98°C), the slides were incubated with primary antibody (1:200) during 1 h at RT. Detection was performed with the UltraMap DAB detection kit (Ventana Medical Systems). Following counterstaining with Mayer's haematoxylin (Dako), the slides were mounted with glass coverslips (Thermo Fisher Scientific) and observed by means of a DM2000 microscope equipped with HC PL Fluotar 20×/0.50 and 40×/0.75 objectives and coupled to a DFC280 CCD camera (Leica Biosystems).

Pathological assessment of ERCC1, PAR, PARP1, and PD-L1 stains as well as evaluation of tumor infiltrating lymphocytes (TILs) were performed independently by a senior pathologist. ERCC1 immunohistochemistry was scored as high or low based on the prominent intensity of

staining observed for each case in the nuclei of tumor cells, as previously described (*32*). Tumors with weak staining (0/1+) were scored as low and tumors with strong staining (2+/3+) were scored as high. PAR and PARP1 expression was evaluated as an H-score (percentage of tumor cells stained multiplied by each intensity from 0 to 3+, value from 0 to 300) as previously described (*57*). PD-L1 expression was evaluated in tumor cells (membranous staining) and immune cells (cytoplasmic or membranous staining) as performed in PD-L1 complementary and companion assays in NSCLC (*58, 59*). TILs density in stromal areas was evaluated as the percentage of stromal areas covered with mononucleated cells whose morphology correspond to lymphocytes, as previously described in other tumor types (*60*).

RNA-Seq

RNA from cells was extracted using the RNeasy mini kit (Qiagen). Initial quality control and quantification of the RNA material was performed using Qubit RNA HS Assay kit on a Qubit 2.0 Fluorometer (Thermo Fisher Scientific). RNA degradation was determined through evaluation of the RIN, using RNA 6000 Pico kit on an Agilent 2100 Bioanalyzer System (Agilent). DNA contamination was then removed using the RNeasy Plus Micro kit (Qiagen). mRNA were isolated using the NEBNext® Poly(A) mRNA magnetic isolation module (New England Biolabs, Ipswich, MA, USA), and library preparation for sequencing was carried out using the NEBNext® Ultra II directional RNA library prep kit for Illumina (New England Biolabs), as per manufacturer's instructions. The completed libraries were then quantified with Tapestation High Sensitivity kit (Agilent) and qPCR using the KAPA Library Quantification kit for Illumina platforms (Kapa Biosystems, Wilmington, MA, USA). The samples were finally clustered using the cBot system (Illumina, San Diego, CA, USA) and sequenced on a HiSeq 2500 platform (Illumina) using a v4 chemistry paired-end flow cell, at 2x100 cycles.

RNA-Seq data analysis

RNA-Seq pre-processing: RNA-Seq generated between 22 and 39 million reads per sample (n = 24). FastQC was used to evaluate library quality and were processed using Trim Galore! version 0.4.5 with cutadapt (*61*) version 1.14 to remove adaptors and trim lower quality reads.

Trimmed reads were aligned to the human reference genome (GRCh38) and gene-level counts were quantified using STAR version 2.5.1b (*62*) in two-pass mode with gene annotations obtained from GENCODE release 22. Post alignment quality control was performed with RseQC (*63*).

RNA-Seq differential expression analysis: Genes with low expression were filtered retaining those with at least 5 counts across 75% of samples. Testing for differential expression was performed using R package edgeR (*64*) version 3.22.0 with the model *~0 + condition + replicate*. Differentially expressed genes were defined as those with a Benjamini-Hocherg adjusted *P*-value of < 0.05 with an absolute $\log_2$ fold change > 0.58 (approximate to a 1.5 fold change in expression).

RNA-Seq downstream analysis: Gene Set Enrichment Analysis (*65*) was performed with fgsea (*66*) version 1.4.1 using the c2.cp.reactome.v6.1 gene set obtained from the Broad Institute with the minimum pathway size set to 10. Genes were ranked according to -$\log_{10}$(adjusted p.value) multiplied by the sign of the $\log_2$ fold change. Significant pathways were defined as those with a Benjamini-Hochberg adjusted *P*-value of < 0.05. The ComBat method implemented in the SVA package (*67*) version 3.26.0 was used to adjust $\log_2$ transformed counts-per-million (CPM) values for the 'replicate' factor in heatmap visualisations. All visualisations were generated in R statistical environment version 3.4.0.

Additional References

57. Michels J, et al. Negative prognostic value of high levels of intracellular poly(ADP-ribose) in non-small cell lung cancer. *Ann Oncol.* 2015;26(12):2470-7.

58. Vennapusa B, et al. Development of a PD-L1 Complementary Diagnostic Immunohistochemistry Assay (SP142) for Atezolizumab. *Appl Immunohistochem Mol Morphol.* 2018.

59. Dolled-Filhart M, et al. Development of a Prototype Immunohistochemistry Assay to Measure Programmed Death Ligand-1 Expression in Tumor Tissue. *Arch Pathol Lab Med.* 2016;140(11):1259-66.

60. Hendry S, et al. Assessing Tumor-Infiltrating Lymphocytes in Solid Tumors: A Practical Review for Pathologists and Proposal for a Standardized Method from the International Immuno-Oncology Biomarkers Working Group: Part 2: TILs in Melanoma, Gastrointestinal Tract Carcinomas, Non-Small Cell Lung Carcinoma and Mesothelioma, Endometrial and Ovarian Carcinomas, Squamous Cell Carcinoma of the Head and Neck, Genitourinary Carcinomas, and Primary Brain Tumors. *Adv Anat Pathol.* 2017;24(6):311-35.

61. Martin M. Cutadapt removes adapter sequences from high-throughput sequencing reads. *EMBnet Journal.* 2011.

62. Dobin A, et al. STAR: ultrafast universal RNA-seq aligner. *Bioinformatics.* 2013;29(1):15-21.

63. Wang L, Wang S, and Li W. RSeQC: quality control of RNA-seq experiments. *Bioinformatics.* 2012;28(16):2184-5.

64. Robinson MD, McCarthy DJ, and Smyth GK. edgeR: a Bioconductor package for differential expression analysis of digital gene expression data. *Bioinformatics.* 2010;26(1):139-40.

65. Subramanian A, et al. Gene set enrichment analysis: a knowledge-based approach for interpreting genome-wide expression profiles. *Proc Natl Acad Sci U S A.* 2005;102(43):15545-50.

66. Sergushichev A. An algorithm for fast preranked gene set enrichment analysis using cumulative statistic calculation. *BioRxiv.* 2016.

67. Leek JT, Johnson WE, Parker HS, Jaffe AE, and Storey JD. The sva package for removing batch effects and other unwanted variation in high-throughput experiments. *Bioinformatics.* 2012;28(6):882-3.